Prediction of the three-phase coexistence line of the ethane hydrate from molecular simulation

Paula Gómez-Álvarez,[1] Miguel J. Torrejón,[1] Jesús Algaba,[1] and Felipe J. Blas*[1]
Laboratorio de Simulación Molecular y Química Computacional, CIQSO-Centro de Investigación en Química Sostenible and Departamento de Ciencias Integradas, Universidad de Huelva, 21006 Huelva Spain

We investigate the three-phase coexistence line of ethane (C_2H_6) hydrate through molecular dynamics simulations using the direct coexistence approach. In this framework, C_2H_6 sI hydrate, aqueous, and pure guest phases are constructed within a single simulation box, allowing us to monitor their mutual stability. From the temporal evolution of the potential energy, we identify the equilibrium temperature (T_3) at which all three phases coexist, across pressures ranging from 1000 to 4000 bar, in accordance with available experimental data. Simulations are performed with the GROMACS package (version 2016, double precision) in the *NPT* ensemble. Water and C_2H_6 molecules are represented using the TIP4P/Ice and TraPPE-UA models, respectively, while unlike non-bonded interactions are computed with the Lorentz–Berthelot combining rule. Dispersive Lennard-Jones and Coulomb interactions are truncated at 1.6 nm, with long-range Coulombic contributions treated via Particle-Mesh Ewald summation. The predicted three-phase coexistence line shows excellent agreement with experimental measurements within the investigated pressure range. These results demonstrate the suitability of the direct coexistence methodology, combined with established molecular models, for reproducing hydrate dissociation behavior in systems that have received little prior computational attention.

*Corresponding author: felipe@uhu.es

I. INTRODUCTION

In the late eighteenth century, several natural philosophers noted the unexpected formation of ice-like solids—even at temperatures above the freezing point of water—when certain gases were bubbled through cold water or when such mixtures were frozen. Sir Humphry Davy was the first scientist to identify these substances as compounds of water and gas, introducing the term "gas hydrates". Following more than a century of continued investigation, these materials were ultimately recognized as clathrates: crystalline frameworks in which small guest molecules are encapsulated within hydrogen-bonded water cages, as exemplified by methane (CH_4) and carbon dioxide (CO_2) under appropriate thermodynamic conditions.[1–3]

Clathrate frameworks also occur in intermetallic compounds,[4,5] where metallic guest ions are enclosed by group 14 (Si, Ge, Sn) frameworks. More recently, clathrate-like assemblies have been realized from colloidal particles,[6,7] enabling larger cages and mesoscale phenomena relevant to biological and photonic systems.

In both gas hydrates and more complex clathrates, host–guest interactions govern stability and functionality, underpinning their utility in natural gas capture[1] and storage.[8] CH_4 hydrates have drawn particular attention as a potential energy resource due to their extensive natural reserves,[1,3,9–16] and as a significant climate factor, acting as a large greenhouse gas reservoir susceptible to destabilization under environmental change.[1,3,9,10,17–19] Additional interest stems from their potential in CO_2 sequestration[20–22] and in gas storage[23] and transport technologies.[24–26]

Accurate knowledge of the thermodynamic stability of gas hydrates is essential for their effective deployment in energy, sequestration, gas storage, and transportation applications. Over recent decades, numerous studies have experimentally determined the hydrate dissociation line, which typically corresponds to a three-phase equilibrium in a two-component system, where hydrate, aqueous, and guest-rich gas or liquid phases coexist—depending on the specific guest molecule involved. Comprehensive discussions can be found in the authoritative monograph by Sloan and Koh,[1] as well as in the recent volume by Ripmeester and Alavi,[3] which offers a detailed review of hydrate phase behavior. From a structural point of view, Matsumoto and Tanaka realized that the arrangement of the guest molecules in the sI and sII hydrate structures is identical to the A15 and C15, respectively, atomic arrangement in the Frank-Kasper structure classification.[27–29] Following this approach, clathrate hydrates can also be viewed from a geometrical perspective, and can be classified as Frank–Kasper structures, which are space-filling packings of "nearly equal" spheres with tetrahedrally close-packed (TCP) topology. This "nearly equal spheres" approach offers a unifying geometrical principle that rationalizes the diversity of hydrate frameworks and provides a natural link between their topological characteristics and the stability trends governed by guest size and occupancy.[28–31]

Molecular simulation is an alternative method to determine the dissociation lines of hydrates.[1,3,32,33] In particular, the direct coexistence method (DC) proposed by Ladd and Woodcock[34,35] was successfully extended to the case of hydrates by Carlos Vega and co-workers,[36,37] who applied it to CH_4. Thanks to the brilliant and pioneering work of Conde and Vega,[36] this approach gave rise to a large number of studies in which the dissociation line of different hydrates was obtained using the direct coexistence method.[36,38–49] Recently, Tanaka and collaborators[50] have proposed an alternative approach, the solubility method, which provides a different route to determine the dissociation lines of hydrates. Several authors have employed this method to predict dissociation lines.[51–55] Hydrate properties including growth, cage occupancy, order parameters, interfacial free energies, and nucleation have also

been addressed through molecular simulation in prior studies.[2,52,56–96]

Although hydrates have diverse applications, including gas separation, transport, and storage, natural gas hydrates attract particular attention due to their significance as an energy resource. The main components of natural gas are CH_4, CO_2, and light linear alkanes such as ethane (C_2H_6). Interestingly, although the dissociation line of C_2H_6 hydrate has been obtained experimentally by several authors,[97–109] to the best of our knowledge, it has not yet been investigated from a molecular perspective.

Gas hydrates generally crystallize into one of three well-characterized structures: sI, sII, or sH. Small guest molecules such as CH_4 and CO_2 typically form sI hydrates while others, including nitrogen (N_2), hydrogen (H_2), and larger species like tetrahydrofuran (THF), more commonly form sII hydrates.[1,3]

The stable structure of C_2H_6 hydrate, as in the case of CH_4 and CO_2 hydrates, is structure sI. The sI unit cell consists of 46 water molecules arranged into two pentagonal dodecahedral (D or 5^{12}) cages and six tetrakaidecahedral (T or $5^{12}6^4$) cages. Under the assumption of single full occupancy, 8 C_2H_6 molecules would occupy all the cages in each unit cell. Until the turn of the twenty-first century, it was generally believed that C_2H_6 molecules occupied only the large T cages, yielding a composition of 6 C_2H_6 molecules per 46 water molecules, i.e., one C_2H_6 molecule per $7.67 \approx 46/6$ water molecules. However, Morita and co-workers demonstrated that molecules can occupy both types of cages.[109] In particular, it had long been assumed that C_2H_6 was too large to fit into the smaller D cages due to the unfavorable ratio of molecular diameter to cage diameter.[1] C_2H_6 hydrate was therefore regarded as a typical clathrate hydrate consisting of filled T cages and empty D cages. Using Raman spectroscopy of the C–C stretching vibration of C_2H_6, Morita et al.[109] showed that C_2H_6 is in fact encapsulated in both T and D cages. The Raman signal corresponding to C–C vibrations in D cages is weak at pressures below 100 MPa, but becomes significant at higher pressures. See Fig. 4 of the work of Morita and collaborators for further details.[109] This provided the first direct spectroscopic evidence of D-cage occupancy by C_2H_6. Following Morita and co-workers, we assume in this work full occupancy in the sI structure of the C_2H_6 hydrate (8 C_2H_6 molecules per 46 water molecules).

The objective of this work is to determine the dissociation line of the hydrate–water–liquid C_2H_6 system over a wide pressure range, using the direct coexistence technique first brilliantly implemented by Carlos Vega and co-workers.[36,37] C_2H_6 hydrate, like some other hydrates, exhibits two dissociation lines: a hydrate–water–liquid ethane line at high pressures and a hydrate–water–vapor ethane line at low pressures. In this study, we focus exclusively on the stable high-pressure branch. Simple but effective models are employed that capture the essential features required for a reliable prediction of the dissociation line: a water model that successfully reproduces the melting point of water at ambient pressure, and a robust ethane model. Specifically, we use the TIP4P/Ice model for water[110] and the TraPPE-UA model for C_2H_6.[111,112]

TABLE I. Non-bonded interaction parameters and geometry details of TIP4P/Ice water[110] and TraPPE-UA C_2H_6[111,112] molecular models employed in this work.

Atom	σ(Å)	ε/k_B(K)	q(e)	Geometry details	
Water (TIP4P/Ice)					
O	3.1668	106.1	-	d_{OH} (Å)	0.9572
H	-	-	0.5897	H–O–H (°)	104.5
M	-	-	-1.1794	d_{OM} (Å)	0.1577
C_2H_6 (TraPPE-UA)					
CH_3	3.75	98.0	-	$d_{CH_3-CH_3}$ (Å)	1.54

The remainder of this paper is organized as follows. Section II presents the molecular models, methodology, and simulation details. The results and their discussion are given in Section III, and the conclusions are summarized in Section IV.

II. MOLECULAR MODELS, METHODOLOGY, AND SIMULATION DETAILS

Molecular dynamics simulations are carried out using the GROMACS software package (version 2016, double precision). Water and ethane molecules are modeled using the well-known TIP4P/Ice[110] and TraPPE-UA[111,112] molecular models. In all cases, the non-bonded unlike interactions are obtained through the Lorentz-Berthelot combination rule, and no extra cross-interaction modification is applied. A summary of the most relevant molecular model details is presented in Table I.

The dispersive Lennard-Jones (LJ) and Coulomb interactions are truncated through a cutoff value of 1.6 nm. Long-range corrections for the dispersive LJ interactions are not applied, but particle-mesh Ewald (PME)[113] corrections are used for the Coulombic potential. Notice that the choice of using a long cutoff value without long-range corrections is far from being arbitrary. As some of the authors of this work have claimed in a previous study, using a small cutoff value could lead to an incorrect prediction of the three-phase dissociation temperature.[47] Although the combination of a small cutoff value and inhomogeneous PME long-range corrections for the LJ dispersive interactions provides a correct estimation of the T_3 value at the same time that reduces the computational cost of the simulations, in this work we decide to use a large cutoff without any long-range correction for the LJ dispersive interactions. The use of a large cutoff value provides the same results as those obtained when long-range corrections are applied.[47] Although the computational cost of the simulations is higher when large cutoff values are used instead of long-range corrections, in GROMACS it is not possible to apply long-range corrections for the LJ dispersive interactions at the same time that the Lorentz-Berthelot combination rule is modified to improve the agreement between experiments and simulations.[39,41,46,47,53–55,95,114,115] For this reason, we have decided to use a large 1.6 nm cutoff value without LJ corrections just in case the Lorentz-Berthelot combination rule must be modified

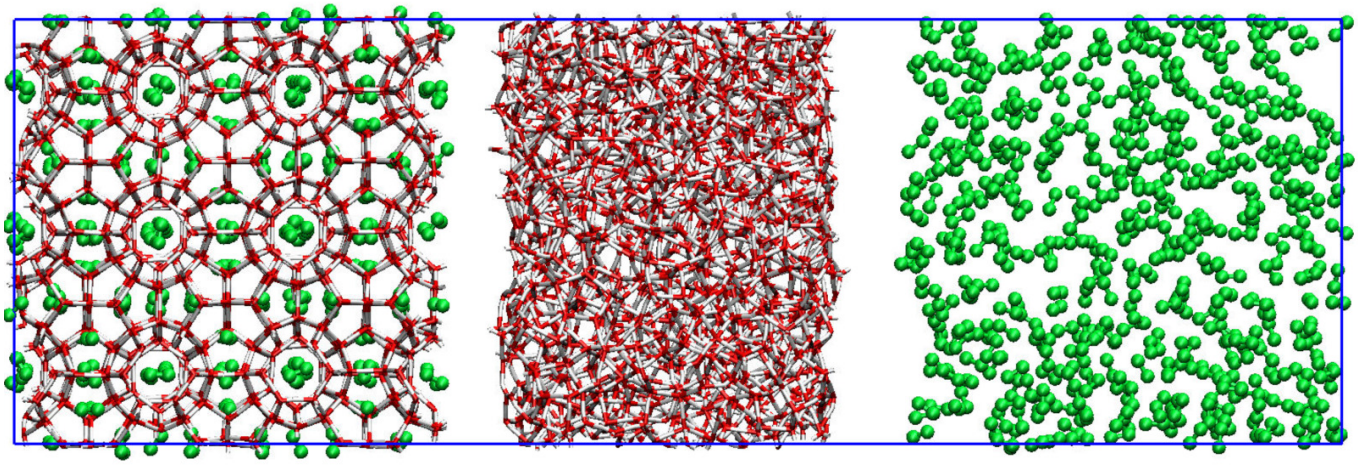

FIG. 1. Representation of the initial simulation box used in this work. green spheres represent the C_2H_6 molecules and red and white licorice representations correspond to water molecules. From left to right, the simulation box is conformed by a hydrate phase, a water phase, and a C_2H_6 phase.

to improve the T_3 predictions.

The T_3 or dissociation temperature of the C_2H_6 sI hydrate is determined from 1000 to 4000 bar using the direct coexistence technique.[34,35,39,40,46,47,116,117] Following this methodology, an initial C_2H_6 sI hydrate, aqueous, and pure guest phases are assembled in the same simulation box, with a central phase surrounded on each side by the other two phases, which allows three-phase coexistence due to periodic boundary conditions. By performing *NPT* simulations, it is possible to determine the temperature at which the three phases coexist. At a certain pressure value, if the temperature fixed during the simulation is higher than the T_3 ($T > T_3$), then the hydrate phase melts since it becomes unstable. On the contrary, if the temperature fixed during the simulation is lower than the T_3 ($T < T_3$), then the hydrate phase grows since the aqueous phase becomes unstable. The T_3 value is determined as the intermediate temperature between the highest T value at which the hydrate phase grows and the lowest T value at which the hydrate phase melts. Uncertainties are estimated by subtracting these two temperatures and dividing by two.[36,39]

To construct the hydrate unit cell, we used the crystallographic parameters reported by Yousuf *et al.*[14] Additionally, the water molecules in C_2H_6 hydrate exhibit proton disorder.[1] To account for this, we generated solid configurations of the sI hydrate using the algorithm developed by Buch *et al.*,[118] which enforces the Bernal–Fowler rules[119] and ensures a net dipole moment that is zero or nearly zero. The initial hydrate phase is then constructed by replicating the C_2H_6 sI hydrate unit cell 3 times ($3 \times 3 \times 3$) in each space direction and assuming full occupancy of the hydrate, i.e., there is a C_2H_6 molecule in each hydrate cage. As a result, the initial hydrate phase contains 1242 molecules of water and 216 molecules of C_2H_6. Then, a pure water phase with 1242 molecules and a pure C_2H_6 guest phase with 400 molecules are added to the simulation box. Based on this setup, the initial configuration consists of a liquid water slab positioned between a solid slab of C_2H_6 hydrate on one side and a slab of liquid C_2H_6 molecules on the other. This arrangement guarantees the coexistence of all three phases under periodic boundary conditions. A schematic of the initial simulation box is presented in Fig. 1.

In all cases, the simulations are run using the *NPT* or isothermal-isobaric ensemble, allowing each side of the simulation box to change independently to keep the pressure constant as well as to avoid any stress from the hydrate solid structure. We use the Verlet-leapfrog[120] algorithm for solving Newton's equations of motion with a time step of 2 fs. In order to keep the temperature and the pressure constant along the simulation, the v-rescale thermostat[121] and the anisotropic Parrinello-Rahman barostat[122] are used with a time constant of 2 ps. In the case of the Parrinello-Rahman barostat, a compressibility value of 4.5×10^{-5} bar^{-1} is applied in the three directions of the simulation box.

III. RESULTS

We have performed simulations at seven different pressures, from 1000 to 4000 bar, to determine the hydrate-water-C_2H_6 three-phase or dissociation line of the C_2H_6 hydrate. According to the DC technique, we simulate a set of temperatures for each pressure to locate the T_3 of the system. Particularly, for each pressure we examine temperature values near the experimental T_3, at a minimum interval of 2 K. This provides a margin of error for T_3 of at least 1 K according to the exposed criterion. As we have already mentioned, each T_3 is estimated as the arithmetic average of the lowest temperature considered at which the ethane hydrate melts and the highest value at which the system freezes, with an uncertainty of 1 K. In all cases, we use the same initial simulation box generated as explained in Section II.

Figure 2 presents the time evolution of the system's potential energy, U, at the lowest pressures examined in this study: 1000, 1500, and 2000 bar. We begin by analyzing the behav-

ior at 1000 bar, shown in Fig. 2a. At this pressure, simulations were conducted at seven temperatures ranging from 292 to 308 K. As observed, the potential energy increases with time at temperatures above 300 K, signaling the dissociation of the C_2H_6 hydrate phase. In contrast, for temperatures below 298 K, the potential energy decreases, indicating crystallization of the hydrate. Based on these trends, the three-phase coexistence temperature, T_3, is estimated to lie between 298 and 300 K. Applying this criterion, the dissociation temperature of the C_2H_6 hydrate at 1000 bar is determined to be 299(1) K, which is in excellent agreement with the experimental value reported in the literature at this pressure, 299.15 K.[1] We have also include these results in Table II.

Three important technical considerations must be addressed. First, although a rigorous statistical approach would require running multiple independent trajectories at each temperature, the computational cost of doing so is prohibitive for the purposes of this study. Given the extensive sampling needed across temperatures and pressures, we opted for single-trajectory simulations at each state point, which still provide valuable qualitative and quantitative insights into phase behavior.

Second, the total simulation time varies depending on the target temperature. As the system approaches the three-phase coexistence temperature, T_3, its dynamics become increasingly stochastic, requiring longer trajectories to capture meaningful trends in the potential energy. For example, at higher temperatures such as 304 and 308 K, the potential energy increases markedly within the first few hundred nanoseconds, consistent with hydrate dissociation. In contrast, for intermediate temperatures such as 296 and 298 K, microsecond-scale simulations are necessary to fully observe the system's evolution: initial trends may suggest hydrate melting, but extended simulations often reveal a reversal in potential energy, indicating hydrate growth. Depending on the thermodynamic conditions, the total simulation time ranges from hundreds of nanoseconds to several microseconds.

Third, the accuracy of the dissociation temperature predictions is supported by the use of the TIP4P/Ice water model,[110] which is specifically parameterized to reproduce the experimental melting point of ice I_h. This choice is critical, as demonstrated in previous studies on CH_4 hydrates,[37] where it was shown that reliable determination of T_3 requires water models that accurately capture the thermodynamics of ice. In the present case, this model contributes significantly to the robustness of our predictions for ethane hydrate.

We now examine the results obtained at the second pressure investigated, 1500 bar, as shown in Fig. 2b. As in the previous case, the system exhibits a decrease in potential energy over time at 296 and 300 K, indicating crystallization of the hydrate phase. In contrast, at the highest temperature considered, 308 K, the potential energy increases sharply, consistent with hydrate dissociation. For the intermediate temperatures between 302 and 306 K, longer simulation times are required to clearly resolve the system's behavior. Based on the observed trends, the three-phase coexistence temperature, T_3, is estimated to lie between 304 and 306 K. From this range, we determine $T_3 = 305(1)$ K, which is in excellent agreement with the experimental value reported at this pressure, 304.15 K.[1] (see also Table II).

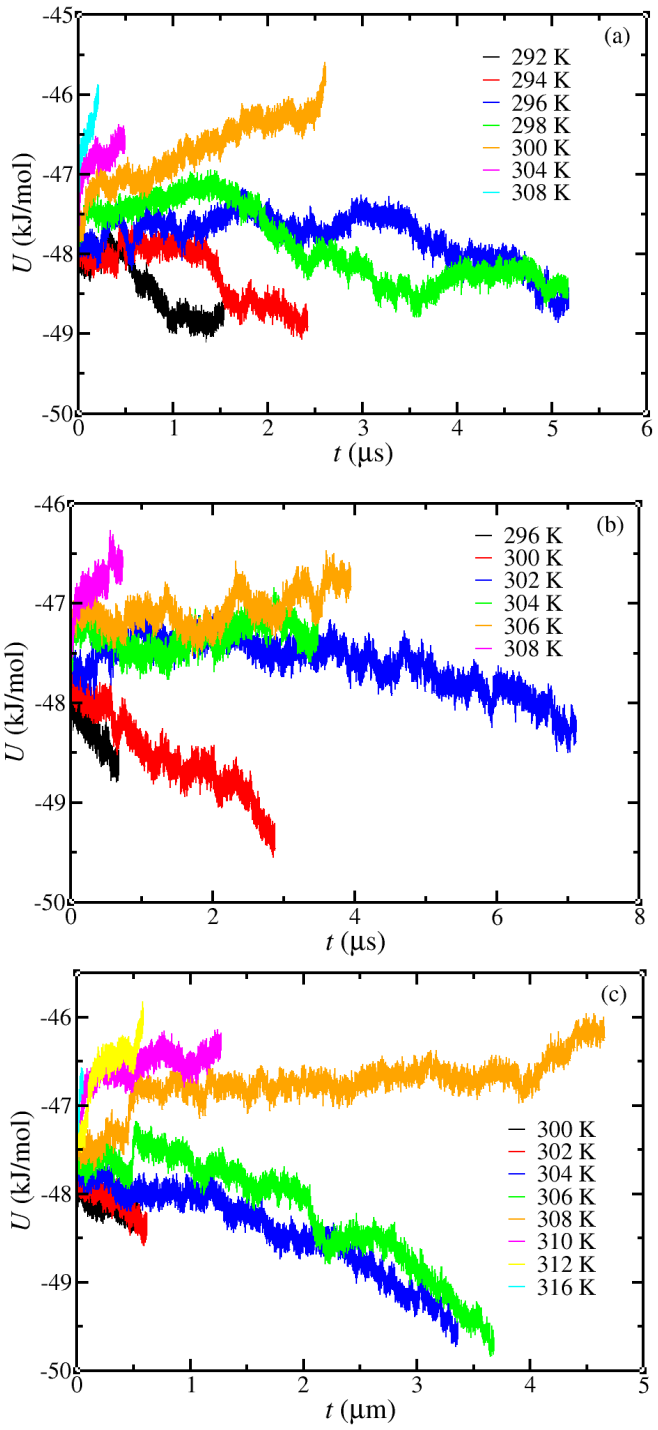

FIG. 2. Evolution of the potential energy as a function of time for the *NPT* runs of the three-phase system at 1000 bar (a),1500 bar (b), and 2000 bar (c) and various temperatures (see legends).

Following the same approach used for the two previous pressures, we analyze the time evolution of the system's potential energy, U, at 2000 bar, as shown in Fig. 2c. Simulations are performed at eight different temperatures. As clearly

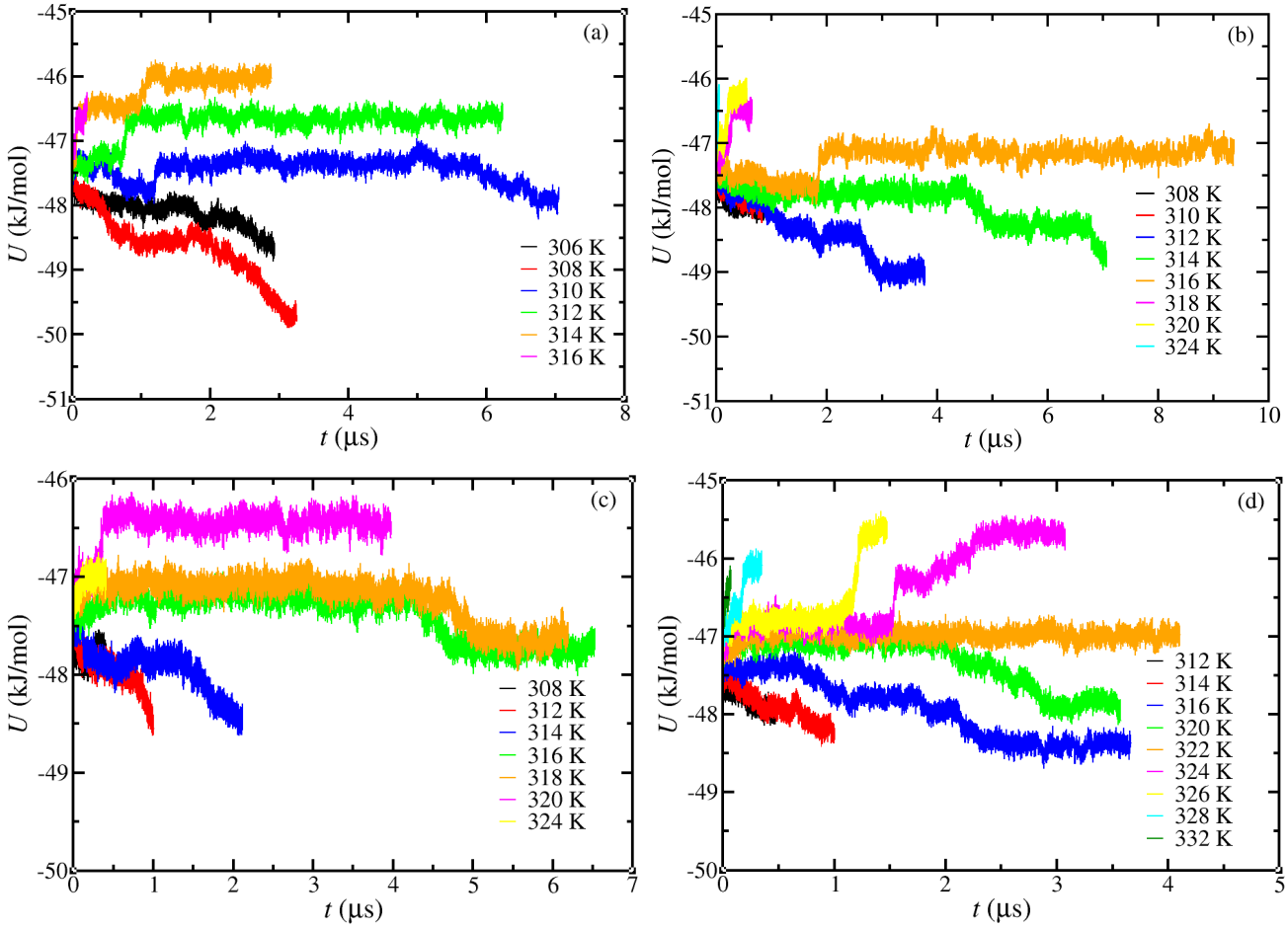

FIG. 3. Evolution of the potential energy as a function of time as obtained from the *NPT* runs of the three-phase system at 2500 (a), 3000 (b), 3500 (c), and 4000 bar (d) and various temperatures (see legends).

observed, the C_2H_6 hydrate phase fully dissociates at temperatures above 308 K, while for temperatures below 306 K, the potential energy decreases over time, indicating the formation of the hydrate phase from liquid water and ethane. Based on these observations, the three-phase coexistence temperature, T_3, is estimated to be 307(1) K, in excellent agreement with the experimental value of 307.26 K.[1] This results is also included in Table II. Notably, at this pressure, the system's energy evolution-whether increasing or decreasing—is more readily distinguishable from the early stages of the simulations, in contrast to the longer onset times required at lower pressures.

Finally, we examine the dissociation behavior of the C_2H_6 hydrate at the highest pressures considered in this study: 2500, 3000, 3500, and 4000 bar. The time evolution of the system's potential energy at various temperatures for each pressure is shown in Fig. 3. As with the lower pressures, a consistent trend is observed: at higher temperatures, the hydrate dissociates, while at lower temperatures, it forms. The dissociation temperature at each pressure lies between these two regimes. Specifically, at 2500 bar, dissociation occurs between 310 (blue) and 312 K (green); at 3000 bar, between 314 (green) and 318 K (orange); at 3500 bar, between 318 (orange) and 320 K (magenta); and at 4000 bar between 320 (green) and 324 K (magenta). From these observations, the estimated three-phase coexistence temperatures are 311(1), 316(2), 319(1), and 322(2) K for 2500, 3000, 3500, and 4000 bar, respectively. All these results have also been included in Table II.

It is worth noting that the estimated uncertainty in the simulated dissociation temperatures is 1 K for all pressures except for 3000 and 4000 bar, where it increases to 2 K. At 3000 bar (Fig. 3b), the three-phase equilibrium temperature lies between 314 K—where the potential energy decreases (green curve)—and 318 K, where it increases (magenta curve). Although simulations were extended to nearly 10μ s, the evolution of the potential energy at 316 K (orange) remained inconclusive, and neither the time series nor the corresponding density profiles provided clear evidence of phase behavior. Consequently, the dissociation temperature at this pressure is estimated to lie within the range of $314 - 318$ K, yielding $T_3 = 316(2)$ K.

At 4000 bar (Fig. 3c), potential energy decreases are observed from the beginning of the simulations at 312 and 314 K,

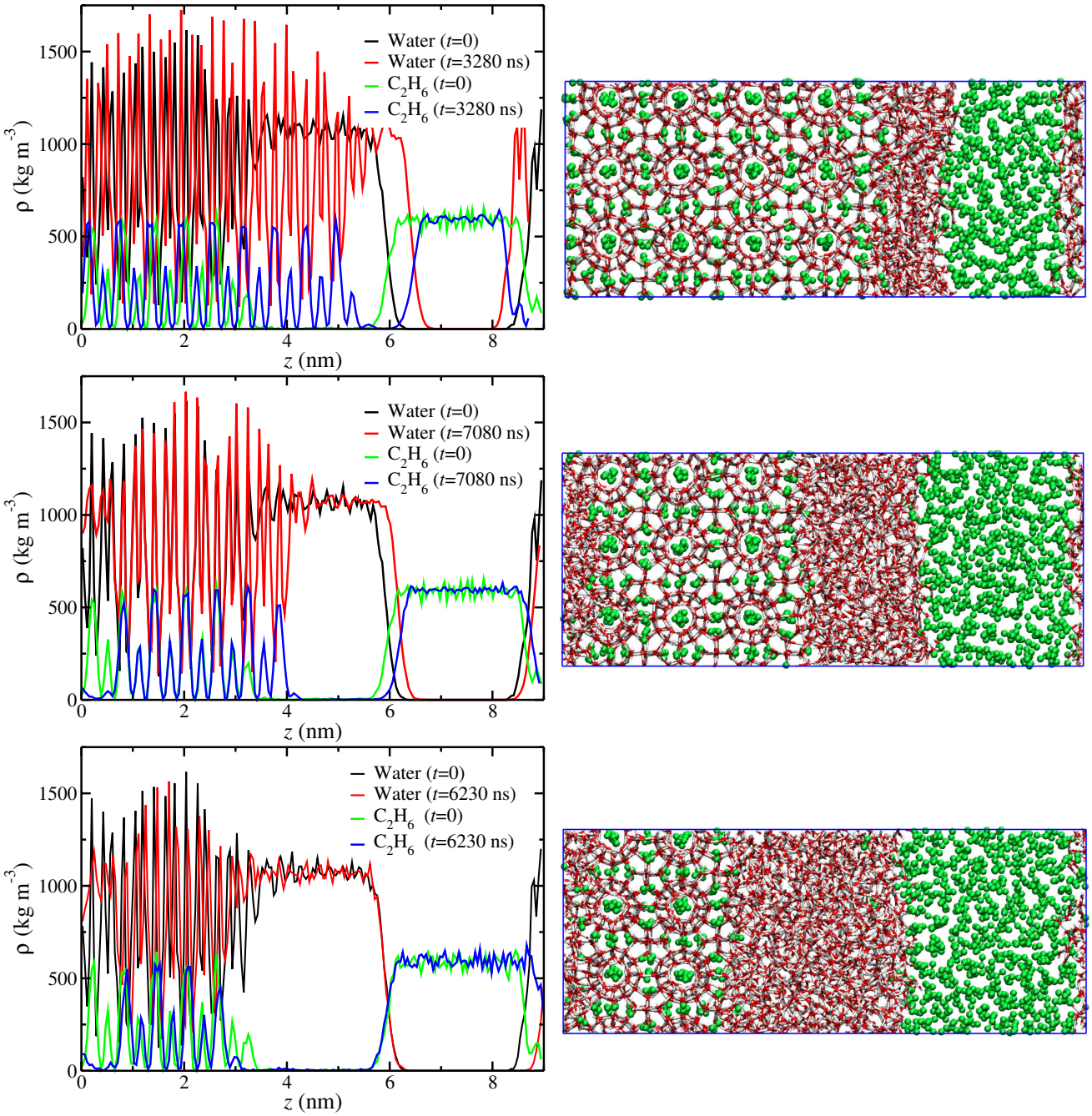

FIG. 4. Ethane and water density profiles and snapshots at 2500 bar at 308 (top), 310 (middle), and 312 K (bottom). The density profiles show the initial and final density distribution of water and C_2H_6 along the simulation box, while the snapshots show the final configuration obtained from the *NPT* simulations.

suggesting hydrate formation. However, for temperatures between 316 and 320 K, longer simulations were required. Beyond 2000 ns, the potential energy decreases for both 316 and 320 K, indicating crystallization, whereas at 322 K, the potential energy remains nearly constant and the density profiles do not clearly indicate either melting or growth. Based on these observations, the dissociation temperature at 4000 bar is estimated as $T_3 = 322(2)$ K.

Having presented the results at each pressure, we now turn to a general analysis of the time evolution of the system's potential energy and its relation to hydrate formation and dissociation across the studied pressure range. Overall, the slope of the decreasing potential energy curves indicates that hydrate growth becomes progressively slower with increasing pressure, suggesting a pressure-dependent kinetic barrier to crystallization. In contrast, hydrate melting tends to occur more rapidly at higher pressures, as evidenced by the earlier onset of energy increases. Additionally, the simulated three-phase

TABLE II. Three-phase dissociation temperatures, T_3, of C_2H_6 hydrate obtained from molecular simulations at various pressures, P. The last column reports the corresponding experimental values, T^{exp}, from the literature.[1]

P (bar)	T (K)	T^{exp} (K)
1000	299 (1)	299.15
1500	305 (1)	304.15
2000	307 (1)	307.26
2500	311 (1)	311.40
3000	316 (2)	314.20
3500	319 (1)	317.49
4000	322 (2)	319.65

coexistence temperatures, T_3, show excellent agreement with experimental data at low and intermediate pressures, while a slight overestimation is observed at the highest pressures investigated.

As previously noted, some of the simulated systems—particularly those at 2500, 3000, and 3500 bar—exhibit significant challenges in reaching equilibrium, complicating the identification of the final state (melting or freezing). To gain deeper insight into the system's evolution under these conditions, we focus on representative simulations of C_2H_6 hydrates at 2500 bar (Fig. 3b). Note that the same procedure has been used for the rest of the pressures in this work. We concentrate on the key temperatures of 308 (red), 310 (blue), and 312 K (green). In order to unambiguously determine whether the system tends toward melting or freezing, we analyze the density profiles of both C_2H_6 and water across the three-phase regions at these selected temperatures, as shown in Fig. 4. To complement this analysis, we also include representative snapshots for each configuration, which illustrate the final state of the system and facilitate a visual comparison. For context, it is helpful to compare these snapshots in Fig. 4 with the initial three-phase configuration shown in Fig. 1.

As shown in Fig. 4, the system exhibits both growth and melting of the hydrate layer, consistent with the trends previously inferred from the potential energy versus time curves. At 308 K (top density profiles and corresponding snapshot), the fluid phases undergo freezing, leading to a clear expansion of the initial ethane hydrate slab. In particular, the number of water and ethane layers in the hydrate phase increases significantly from the initial configuration (black and green curves) to the final stage of the simulation (red and blue curves). Initially, the hydrate–water interface is located at approximately 3.5 nm, but after 3.2μs, it has advanced to around 6 nm. Concurrently, the water-rich phase, initially spanning from 3.5 to 5.5 nm, has contracted to a width of about 1 nm or less. The ethane-rich liquid phase also exhibits a slight reduction in size, although to a lesser extent, as reflected in the density profiles. This behavior is further corroborated by the visual comparison of the final system snapshot at 312 K (top panel in Fig. 4) with the initial three-phase configuration (Fig. 1). The hydrate phase has clearly expanded—with the formation of an additional layer composed of large or T cages and some small or D cages—while the liquid water and ethane phases have notably diminished, especially the water phase.

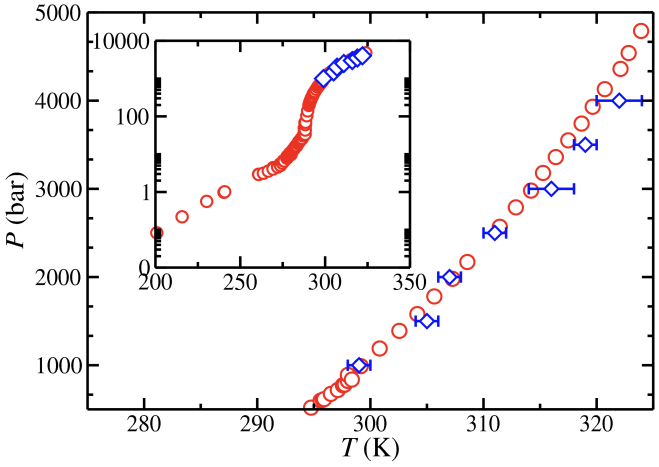

FIG. 5. Pressure-temperature projection of the dissociation line of the C_2H_6 hydrate. Blue diamonds are the results obtained in this work using the direct coexistence method, the TIP4P/Ice model for water, and the TraPPE model for C_2H_6. Red circles correspond to experimental data taken from the literature.[97–109]

At 312 K, the system exhibits a markedly different behavior, as shown in the lower density profiles and corresponding snapshot. The hydrate phase undergoes dissociation, resulting in a noticeable reduction of the initial hydrate slab. This is evidenced by the decrease in the number of water and ethane layers from the initial configuration (black and green curves) to the final state (red and blue curves). Over the course of the 6.2μs simulation, the hydrate–water interface shifts from approximately 3.5 to 2.5 nm, indicating the retreat of the solid phase. Simultaneously, the water-rich region expands from an initial width of 2 to about 3 nm, while the ethane-rich liquid phase also grows slightly. These structural changes are further supported by the final system snapshot (bottom panel, Fig. 4), which shows the contraction of the hydrate and the corresponding expansion of the surrounding fluid phases. Notably, a layer composed of large (T) cages and some small (D) cages disappears, highlighting the breakdown of the crystalline structure.

The middle density profiles and corresponding snapshot in Fig. 4 depict the final configuration obtained at 312 K. As indicated by the potential energy evolution in Fig. 3a (blue curve), the system exhibits a net decrease in energy over time, suggesting hydrate growth. Although the structural changes are less pronounced than those observed at 308 K, both the density profiles and the snapshot provide evidence of hydrate formation. Specifically, the water density profile (red curves) shows increased structuring, and the snapshot reveals the early development of a hydrate layer, originating from a thin layer of small (D) cages at the hydrate–water interface. Considering that the hydrate melts at 312 and grows at 310 K, the three-phase coexistence temperature is estimated as 311(1) K, in excellent agreement with the experimental value of 311.4 K.[1] This conclusion is consistent with the interpretation of the potential energy curves in Fig. 3b.

As it has been commented previously, Morita and co-

workers demonstrated that C_2H_6 molecules can occupy both types of cages[109] although it had long been assumed that C_2H_6 was too large to fit into the smaller D cages, and only the big T cages are filled.[1] In this work, and following the work of Morita *et al.*,[109] the initial hydrate seed is fully occupied. However, from the analysis of the density profiles of those simulations where the hydrate phase grows, it is possible to analyze the occupancy of the new-growth hydrate. The C_2H_6/water molecule ratio in a fully occupied hydrate is 8/46, where 6 C_2H_6 molecules occupy the large T cages and 2 C_2H_6 molecules occupy the small D cages. If only the large T cages of the new-growth hydrate are occupied by C_2H_6 molecules, while the small D cages remain empty, the C_2H_6/water molecule ratio would be 6/46. In this work, we have analyzed the density at one temperature at the lowest pressure (1000 bar), an intermediate pressure (2500 bar), and the highest pressure (4000 bar). From these pressures, we have selected the density profile with the highest expansion of the hydrate phase from the different simulated temperatures. This is done in order to ensure that the new-growth hydrate phase is large enough to provide enough statistics about the number of C_2H_6 and water molecules. In particular, we have analyzed the density profiles at 1000 bar and 298 K, 2500 bar and 308 K, and 4000 bar and 320 K. The C_2H_6/water molecule ratios of the new-growth hydrate obtained at these conditions are 7.8/46, 8.2/46, and 7.9/46. Notice that in all cases, we can round the C_2H_6/water molecule ratio to 8/46, which corresponds to a fully occupied sI hydrate as Morita *et al.*[109] claimed in their experimental work. However, these calculations have to be considered just as a first approximation to understand the effect of the occupancy of the small D cages, and further work is required to understand it fully. A more rigorous determination of the hydration number of hydrates is possible,[123–126] but this lies beyond the scope of the present work.

Finally, the dissociation line of C_2H_6 hydrate obtained from molecular simulations is summarized in the pressure–temperature phase diagram shown in Fig. 5. For comparison, experimental data from the literature covering the entire pressure range studied are also included.[97–109] It is interesting to note that the C_2H_6-water phase diagram shows two quadrupole points.[1] The first (lower) quadrupole point, Q_1, occurs at 272.9 K and 25.6 bar. Under these conditions, there exist four phases in equilibrium: a hydrate phase, an ice Ih phase, a water-rich liquid phase, and a vapor phase. The second (upper) quadrupole point, Q_2, occurs at 287.8 K and 33.9 bar. Under these conditions, there exist four phases in equilibrium: a hydrate phase, a water-rich liquid phase, a C_2H_6-rich liquid phase, and a vapor phase. The changes in slope occur precisely under these thermodynamic conditions, corresponding to the ice Ih–to–water-rich phase transition and the vapor–liquid transition of the C_2H_6-rich phase. As observed, the simulated dissociation line agrees well with the experimental results, with all values falling within the estimated statistical uncertainties reported throughout the text. Notably, both the simulated and experimental curves exhibit similar slopes, indicating that the agreement is not only quantitative but also qualitative.

IV. CONCLUSIONS

In this work, we have carried out molecular dynamics simulations employing the direct coexistence method to determine the three-phase (hydrate–water–ethane) coexistence line of the C_2H_6 hydrate system. Simulations are performed at pressures ranging from 1000 to 4000 bar. The predicted dissociation temperatures, T_3, show very good agreement with experimental data across the entire pressure range, with only slight overestimations observed at the highest pressures. These results highlight the reliability of the employed methodology and interaction models in capturing the phase behavior of this computationally underexplored system. Specifically, the combination of the TIP4P/Ice water model with the TraPPE force field for ethane, using Lorentz–Berthelot combining rules for cross interactions, proves to be a robust and accurate choice. No adjustments to the standard combining rules or inclusion of long-range Lennard-Jones corrections are necessary to achieve quantitative agreement. Additionally, we find that the simulation time required to observe phase transitions strongly depends on the proximity to the dissociation temperature: significantly longer trajectories are needed when the system is near T_3, due to the increasingly slow dynamics near equilibrium.

ACKNOWLEDGEMENTS

The authors wish to dedicate this work and express their heartfelt gratitude to our friend Prof. Carlos Vega for his invaluable contributions to the study of complex systems by computer simulation, and in particular for his efforts to understand the properties of water from a molecular perspective, including hydrate clathrates. The development of simplified yet accurate water models over the past decades has been fundamental to advancing microscopic knowledge of aqueous systems, providing deeper insight into their structure and behavior. His legacy continues to guide both theoretical and applied research, inspiring future generations of scientists not only in Spain but throughout the world. We deeply value his tireless dedication and the enduring impact of his contributions to science. In the group at the University of Huelva, we are deeply grateful for your sincere friendship, which goes beyond scientific cordiality and reaches a personal level. Carlos, you know that you are always welcome in Huelva by all of us and by the V. de R. We acknowledge Grant Refs (PID2021-125081NB-I00 and PID2024-158030NB-I00) financed both by MCIN/AEI/10.13039/501100011033 and FEDER EU, and Universidad de Huelva (P.O. FEDER EPIT1282023), also cofinanced by EU FEDER funds. M.J.T. acknowledges the research contract (Ref 01/2022/38143) of Programa Investigo (Plan de Recuperación, Transformación y Resiliencia, Fondos NextGeneration EU) from Junta de Andalucía (HU/INV/0004/2022). Part of the computations was carried out at the Centro de Supercomputación de Galicia (CESGA, www.cesga.es, Finisterrae III Supercomputer). We also greatly acknowledge RES resources provided by the Barcelona Supercomputing Center in Mare Nostrum to FI-2025-2-0032.

AUTHOR DECLARATIONS

Conflict of interests

The authors declare no conflicts to disclose.

AUTHOR CONTRIBUTIONS

Paula Gómez-Álvarez: Methodology (equal); Investigation (lead); Writing – original draft (equal); Writing – review & editing (equal).**Miguel J. Torrejón:** Methodology (equal); Writing – original draft (equal); Writing – review & editing (equal). **Jesús Algaba:** Methodology (equal); Writing – original draft (equal); Writing – review & editing (equal). **Felipe J. Blas:** Conceptualization (lead); Funding acquisition (lead); Methodology (equal); Writing – original draft (equal); Writing – review & editing (equal).

DATA AVAILABILITY

The data that support the findings of this study are available within the article.

[1] E. D. Sloan and C. Koh, *Clathrate Hydrates of Natural Gases*, 3rd ed. (CRC Press, New York, 2008).

[2] B. C. Barnes and A. K. Sum, "Advances in molecular simulations of clathrate hydrates," Curr. Opin. Chem. Eng. **2**, 184–190 (2013).

[3] J. A. Ripmeester and S. Alavi, *Clathrate Hydrates: Molecular Science and Characterization* (Wiley-VCH: Weinheim, Germany, 2022).

[4] J.-A. Dolyniuk, B. Owens-Baird, J. Wang, J. V. Zaikina, and K. Kovnir, "Clathrate thermoelectrics," Mater. Sci. Eng. R. Rep. **108**, 1–46 (2016).

[5] J. S. Kasper, P. Hagenmuller, M. Pouchard, and C. Cros, "Clathrate structure of silicon Na_8Si_{46} and Na_xSi_{136} $(x < 11)$," Science **150**, 1713–1714 (1965).

[6] H. Lin, S. Lee, L. Sun, M. Spellings, M. Engel, S. C. Glotzer, and C. A. MirkinX, "Clathrate colloidal crystals," Science **355**, 931–935 (2017).

[7] S. Lee, E. G. Teich, M. Engel, and S. C. Glotzer, "Entropic colloidal crystallization pathways via fluid–fluid transitions and multidimensional prenucleation motifs," Proc. Natl Acad. Sci. USA **116**, 14843–14851 (2019).

[8] W. L. Mao, H. K. Mao, A. F. Goncharov, V. V. Struzhkin, Q. Guo, J. Hu, J. Shu, R. J. Hemley, M. Somayazulu, and Y. Zhao, "Hydrogen clusters in clathrate hydrate," Science **297**, 2247–2249 (2002).

[9] E. D. Sloan, "Fundamental principles and applications of natural gas hydrates," Science **426**, 353–359 (2003).

[10] C. A. Koh, A. K. Sum, and E. D. Sloan, "State of the art: Natural gas hydrates as a natural resource," J. Nat. Gas Sci. Eng. **8**, 132–138 (2012).

[11] Z. R. Chong, S. H. B. Yang, P. Babu, P. Linga, and X.-S. Li, "Review of natural gas hydrates as an energy resource: Prospects and challenges," Appl. Energy **162**, 1633–1652 (2016).

[12] J. Zheng, Z. R. Chong, M. F. Qureshi, and P. Linga, "Carbon dioxide sequestration via gas hydrates: a potential pathway toward decarbonization," Energy & Fuels **34**, 10529–10546 (2020).

[13] C. Bourry, J.-L. Charlou, J.-P. Donval, M. Brunelli, C. Focsa, and B. Chazallon, "X-ray synchrotron diffraction study of natural gas hydrates from african margin," Geophysical Research Letters **34** (2007).

[14] M. Yousuf, S. Qadri, D. Knies, K. Grabowski, R. Coffin, and J. Pohlman, "Novel results on structural investigations of natural minerals of clathrate hydrates," Applied Physics A **78**, 925–939 (2004).

[15] Y. F. Makogon, *Hydrates of hydrocarbons* (PennWell Publishing Co., Tulsa, OK, 1997).

[16] H. Aghajari, M. H. Moghaddam, and M. Zallaghi, "Study of effective parameters for enhancement of methane gas production from natural gas hydrate reservoirs," Green Energy & Environment **4**, 453–469 (2019).

[17] A. Y. Manakov, S. V. Goryainov, A. V. Kurnosov, A. Y. Likhacheva, Y. A. Dyadin, and E. G. Larionov, "Clathrate nature of the high-pressure tetrahydrofuran hydrate phase and some new data on the phase diagram of the tetrahydrofuran-water system at pressures up to 3 GPa," J. Phys. Chem. B **107**, 7861–7866 (2003).

[18] T. Makino, T. Sugahara, and K. Ohgaki, "Stability boundaries of tetrahydrofuran + water system," J. Chem. Eng. Data **50**, 2058–2060 (2005).

[19] K. A. Kvenvolden, "Methane hydrate – a major reservoir of carbon in the shallow geosphere?" Chem. Geol. **71**, 41–51 (1988).

[20] S. Choi, J. H. Drese, and C. W. Jones, "Methane exploitation by carbon dioxide from gas hydrates—phase equilibria for CO_2-CH_4 mixed hydrate system," J. Chem. Eng. Jpn. **29**, 478–483 (1996).

[21] M. Yand, Y. Song, L. Jiang, Y. Zhao, X. Ruan, Y. Zhang, and S. Wang, "Hydrate-based technology for CO_2 capture from fossil fuel power plants," Appl. Energy **116**, 26–40 (2014).

[22] M. Ricaurte, C. Dicharry, X. Renaud, and J.-P. Torré, "Combination of surfactants and organic compounds for boosting CO_2 separation from natural gas by clathrate hydrate formation," Fuel **122**, 206–217 (2014).

[23] B. Kvamme, G. A, T. Buanes, T. Kuznetsova, and G. Ersland, "Storage of CO_2 in natural gas hydrate reservoirs and the effect of hydrate as an extra sealing in cold aquifers," Int. J. Greenhouse Gas Control **1**, 236–246 (2007).

[24] V. Chihaua, S. Adams, and W. F. Kuhs, "Molecular dynamics simulations of properties of a (001) methane clathrate hydrate surface," Chem. Phys. **317**, 208–225 (2005).

[25] B. Peters, N. E. R. Zimmermann, G. T. Beckham, J. W. Tester, and B. J. Trout, "Path sampling calculation of methane diffusivity in natural gas hydrates from a water-vacancy assisted mechanism," J. Am. Chem. Soc. **130**, 17342–17350 (2008).

[26] N. J. English and J. S. Tse, "Mechanisms for thermal conduction in methane hydrate," Phys. Rev. Lett. **103**, 015901 (2009).

[27] F. C. Frank and J. S. Kasper, "Complex alloy structures regarded as sphere packings. i. definitions and basic principles," Acta Crystallographica **11**, 184–190 (1958).

[28] M. Matsumoto and H. Tanaka, "On the structure selectivity of clathrate hydrates," The Journal of Physical Chemistry B **115**, 8257–8265 (2011).

[29] M. Matsumoto and H. Tanaka, "Structure selectivity of mixed gas hydrates and group 14 clathrates," Energy & Fuels **36**, 10667–10674 (2022).

[30] S. Muromachi and S. Takeya, "Discovery of the final primitive frank-kasper phase of clathrate hydrates," Science Advances **10**, eadp4384 (2024).

[31] Y. Chen, S. Takeya, and A. K. Sum, "Topological dual and extended relations between networks of clathrate hydrates and frank-kasper phases," Nature Communications **14**, 596 (2023).

[32] M. P. Allen and D. J. Tildesley, *Computer Simulation of Liquids, 2nd Ed.* (Claredon, Oxford, 2017).

[33] D. Frenkel and B. Smit, *Understanding Molecular Simulations* (2nd Ed. Academic, San Diego, 2002).

[34] J. C. Ladd and L. V. Woodcock, "Triple-point coexistence properties of the Lennard-Jones system," Chem. Phys. Lett. **51**, 155–159 (1977).

[35] J. C. Ladd and L. V. Woodcock, "Interfacial and co-existence properties of the lennard-jones system at the triple point," Mol. Phys. **36**, 611 (1978).

[36] M. M. Conde and C. Vega, "Determining the three-phase coexistence line in methane hydrates using computer simulations," J. Chem. Phys. **133**, 064507 (2010).

[37] M. M. Conde and C. Vega, "Note: A simple correlation to locate the three phase coexistence line in methane-hydrate simulations," J. Chem. Phys. **138**, 056101 (2013).

[38] L. Jensen, K. Thomsen, N. von Solms, S. Wierzchowski, M. R. Walsh, C. A. Koh, E. D. Sloan, D. T. Wu, and A. K. Sum, "Calculation of liquid water–hydrate–methane vapor phase equilibria from molecular simulations," J. Phys. Chem. B **114**, 5775–5782 (2010).

[39] J. M. Míguez, M. M. Conde, J.-P. Torré, F. J. Blas, M. M. Piñeiro, and C. Vega, "Molecular dynamics simulation of CO_2 hydrates: Prediction of three phase coexistence line," J. Chem. Phys. **142**, 124505 (2015).

[40] V. K. Michalis, J. Costandy, I. N. Tsimpanogiannis, A. K. Stubos, and I. G. Economou, "Prediction of the phase equilibria of methane hydrates using the direct phase coexistence methodology," J. Chem. Phys. **142**, 044501 (2015).

[41]J. Costandy, V. K. Michalis, I. N. Tsimpanogiannis, A. K. Stubos, and I. G. Economou, "The role of intermolecular interactions in the prediction of the phase equilibria of carbon dioxide hydrates," J. Chem. Phys. **143**, 094506 (2015).
[42]M. Pérez-Rodríguez, A. Vidal-Vidal, J. Míguez, F. J. Blas, J.-P. Torré, and M. M. Piñeiro, "Computational study of the interplay between intermolecular interactions and CO_2 orientations in type I hydrates," Phys. Chem. Chem. Phys. **19**, 3384–3393 (2017).
[43]A. M. Fernández-Fernández, M. Pérez-Rodríguez, A. Comesaña, and M. M. Piñeiro, "Three-phase equilibrium curve shift for methane hydrate in oceanic conditions calculated from molecular dynamics simulations," J. Mol. Liq. **274**, 426–433 (2019).
[44]A. M. Fernández-Fernández, M. M. Piñeiro, and M. Pérez-Rodríguez, "Molecular dynamics of fluoromethane type I hydrates," J. Mol. Liq. **339**, 116720 (2021).
[45]S. Blazquez, C. Vega, and M. M. Conde, "Three phase equilibria of the methane hydrate in NaCl solutions: A simulation study," J. Mol. Liq. **383**, 122031 (2023).
[46]J. Algaba, S. Blazquez, E. Feria, J. M. Míguez, M. M. Conde, and F. J. Blas, "Three-phase equilibria of hydrates from computer simulation. II: Finite-size effects in the carbon dioxide hydrate," J. Chem. Phys. **160**, 164722 (2024).
[47]J. Algaba, S. Blazquez, J. M. Míguez, M. M. Conde, and F. J. Blas, "Three-phase equilibria of hydrates from computer simulation. III: Effect of dispersive interactions in methane and carbon dioxide hydrates," J. Chem. Phys. **160**, 164723 (2024).
[48]A. Borrero, A. Díaz-Acosta, S. Blazquez, I. M. Zerón, J. Algaba, M. M. Conde, and F. J. Blas, "Three-phase equilibria of CO_2 hydrate from computer simulation in the presence of NaCl," Energy Fuels **39**, 5522–5533 (2025).
[49]M. J. Torrejón, S. Blazquez, J. Algaba, M. M. Conde, and F. J. Blas, "Dissociation line and driving force for nucleation of the multiple occupied hydrogen hydrate from computer simulation," Energy Fuels **39**, 15184–15197 (2025).
[50]H. Tanaka, T. Yagasaki, and M. Matsumoto, "On the thermodynamic stability of clathrate hydrates VI: complete phase diagram," The Journal of Physical Chemistry B **122**, 297–308 (2018).
[51]J. Grabowska, S. Blázquez, E. Sanz, I. M. Zerón, J. Algaba, J. M. Míguez, F. J. Blas, and C. Vega, "Solubility of methane in water: some useful results for hydrate nucleation," J. Phys. Chem. B **126**, 8553–8570 (2022).
[52]J. Grabowska, S. Blázquez, E. Sanz, E. G. Noya, I. M. Zerón, J. Algaba, J. M. Míguez, F. J. Blas, and C. Vega, "Homogeneous nucleation rate of methane hydrate formation under experimental conditions from seeding simulations," J. Chem. Phys. **158**, 114505 (2023).
[53]J. Algaba, I. M. Zerón, J. M. Míguez, J. Grabowska, S. Blazquez, E. Sanz, C. Vega, and F. J. Blas, "Solubility of carbon dioxide in water: Some useful results for hydrate nucleation," J. Chem. Phys. **158**, 054505 (2023).
[54]J. Algaba, M. J. Torrejón, and F. J. Blas, "Dissociation line and driving force for nucleation of the nitrogen hydrate from computer simulation," J. Chem. Phys. **159**, 224707 (2023).
[55]M. J. Torrejón, J. Algaba, and F. J. Blas, "Dissociation line and driving force for nucleation of the nitrogen hydrate from computer simulation. II. effect of multiple occupancy," J. Chem. Phys. **161**, 054712 (2024).
[56]S. Alavi, J. A. Ripmeester, and D. D. Klug, "Molecular-dynamics study of structure II hydrogen clathrates," J. Chem. Phys. **123**, 024507 (2005).
[57]S. Alavi, J. A. Ripmeester, and D. D. Klug, "Molecular-dynamics simulations of binary structure II hydrogen and tetrahydrofurane clathrates," J. Chem. Phys. **124**, 014704 (2006).
[58]S. Alavi and J. A. Ripmeester, "Hydrogen-gas migration through clathrate hydrate cages," Angewandte Chemie **119**, 6214–6217 (2007).
[59]I. M. Zerón, J. Algaba, J. M. Míguez, J. Grabowska, S. Blazquez, E. Sanz, C. Vega, and F. J. Blas, "Homogeneous nucleation rate of carbon dioxide hydrate formation under experimental condition from seeding simulations," J. Chem. Phys. **162**, 134708 (2025).
[60]J. Algaba, E. Acuña, J. M. Míguez, B. Mendiboure, I. M. Zerón, and F. J. Blas, "Simulation of the carbon dioxide hydrate-water interfacial energy," J. Colloid Interf. Sci. **623**, 354–367 (2022).
[61]I. M. Zerón, J. M. Míguez, B. Mendiboure, J. Algaba, and F. J. Blas, "Simulation of the CO_2 hydrate–water interfacial energy: The mold integration–guest methodology," J. Chem. Phys. **157**, 134709 (2022).
[62]C. Romero-Guzmán, I. M. Zerón, J. Algaba, B. Mendiboure, J. M. Míguez, and F. J. Blas, "Effect of pressure on the carbon dioxide hydrate–water interfacial free energy along its dissociation line," J. Chem. Phys. **158**, 194704 (2023).
[63]M. J. Torrejón, C. Romero-Guzmán, M. M. Piñeiro, F. J. Blas, and J. Algaba, "Simulation of the THF hydrate - water interfacial free energy from computer simulation," J. Chem. Phys. **161**, 064701 (2024).
[64]I. M. Zerón, J. Algaba, J. M. Míguez, B. Mendiboure, and F. J. Blas, "Rotationally invariant local bond order parameters for accurate determination of hydrate structures," Molecular Physics **122**, e2395438 (2024).
[65]B. R. García, J. Algaba, F. J. Blas, M. Pérez-Rodríguez, and M. M. Piñeiro, "Monitoring hydroquinone clathrates in molecular simulation using local bond order parameters," Energy Fuels **39**, 9884–9892 (2025).
[66]R. S. DeFever and S. Sarupria, "Nucleation mechanism of clathrate hydrates of water-soluble guest molecules," J. Chem. Phys. **147** (2017).
[67]P. E. Brumby, D. Yuhara, D. T. Wu, A. K. Sum, and K. Yasuoka, "Cage occupancy of methane hydrates from gibbs ensemble monte carlo simulations," Fluid Phase Equilibr. **413**, 242–248 (2016).
[68]P. E. Brumby, D. Yuhara, T. Hasegawa, D. T. Wu, A. K. Sum, and K. Yasuoka, "Cage occupancies, lattice constants, and guest chemical potentials for structure II hydrogen clathrate hydrate from Gibbs ensemble Monte Carlo simulations," J. Chem. Phys. **150**, 134503 (2019).
[69]Y. Krishnan, P. G. Rosingana, M. R. Ghaani, and N. J. English, "Controlling hydrogen release from remaining-intact clathrate hydrates by electromagnetic fields: molecular engineering via microsecond non-equilibrium molecular dynamics," RSC advances **12**, 4370–4376 (2022).
[70]S. A. Bagherzadeh, S. Alavi, J. Ripmeester, and P. Englezos, "Formation of methane nano-bubbles during hydrate decomposition and their effect on hydrate growth," J. Chem. Phys. **142**, 214701 (2015).
[71]K. Katsumasa, K. Koga, and H. Tanaka, "On the thermodynamic stability of hydrogen clathrate hydrates," J. Chem. Phys. **127** (2007).
[72]P. Cao, F. Ning, J. Wu, B. Cao, T. Li, H. A. Sveinsson, Z. Liu, T. J. Vlugt, and M. Hyodo, "Mechanical response of nanocrystalline ice-contained methane hydrates: Key role of water ice," ACS Appl. Mater. Interfaces **12**, 14016–14028 (2020).
[73]L. Hakim, K. Koga, and H. Tanaka, "Thermodynamic stability of hydrogen hydrates of ice I_c and II structures," Phys. Rev. B **82**, 144105 (2010).
[74]T. Nakayama, K. Koga, and H. Tanaka, "Augmented stability of hydrogen clathrate hydrates by weakly polar molecules," J. Chem. Phys. **131** (2009).
[75]B. Fang, F. Ning, P. Cao, L. Peng, J. Wu, Z. Zhang, T. J. Vlugt, and S. Kjelstrup, "Modeling thermodynamic properties of propane or tetrahydrofuran mixed with carbon dioxide or methane in structure-II clathrate hydrates," J. Phys. Chem. C **121**, 23911–23925 (2017).
[76]B. Fang, O. Moultos, T. L. J. Sun, Z. Liu, F. Ning, and T. J. H. Vlugt, "Effects of nanobubbles on methane hydrate dissociation: A molecular simulation study," Fuel **345**, 128230 (2023).
[77]B. Fang, T. Lü, W. Li, O. A. Moultos, T. J. Vlugt, and F. Ning, "Microscopic insights into poly-and mono-crystalline methane hydrate dissociation in Na-montmorillonite pores at static and dynamic fluid conditions," Energy **288**, 129755 (2024).
[78]M. Matsuo, Y. Takii, M. Matsumoto, and H. Tanaka, "On the occupancy of carbon dioxide clathrate hydrates: Grandcanonical monte carlo simulations," J. Phys. Soc. Jpn. **81**, SA027–1 (2012).
[79]T. Yagasaki, M. Matsumoto, Y. Andoh, S. Okazaki, and H. Tanaka, "Effect of bubble formation on the dissociation of methane hydrate in water: A molecular dynamics study," J. Phys. Chem. B **118**, 1900 (2014).
[80]M. R. Walsh, G. T. Beckham, C. A. Koh, E. D. Sloan, D. T. Wu, and A. K. Sum, "Methane hydrate nucleation rates from molecular dynamics simulations: Effects of aqueous methane concentration, interfacial curvature, and system size," J. Phys. Chem. C **115**, 21241 (2011).
[81]B. C. Knott, V. Molinero, M. F. Doherty, and B. Peters, "Homogeneous nucleation of methane hydrates: Unrealistic under realistic conditions," J. Am. Chem. Soc. **134**, 19544–19547 (2012).
[82]B. C. Barnes, B. C. Knott, G. T. Beckham, D. Wu, and A. K. Sum, "Molecular dynamics study of carbon dioxide hydrate dissociation," J. Phys. Chem. B **118**, 13236–13243 (2014).
[83]B. C. Barnes, B. C. Knott, G. T. Beckham, D. T. Wu, and A. K. Sum, "Reaction coordinate of incipient methane clathrate hydrate nucleation," J. Phys. Chem. B. **118**, 13236–13243 (2014).

[84]L. C. Jacobson, W. Hujo, and V. Molinero, "Amorphous precursors in the nucleation of clathrate hydrates," J. Am. Chem. Soc. **132**, 11806–11811 (2010).
[85]L. C. Jacobson, W. Hujo, and V. Molinero, "Nucleation pathways of clathrate hydrates: Effect of guest size and solubility," J. Phys. Chem. B **114**, 13796–13807 (2010).
[86]L. C. Jacobson, W. Hujo, and V. Molinero, "Nucleation pathways of clathrate hydrates: Effect of guest size and solubility," J. Phys. Chem. B **114**, 13796–13807 (2010).
[87]L. C. Jacobson and V. Molinero, "A methane-water model for coarse-grained simulations of solutions and clathrate hydrates," J. Phys. Chem. B **114**, 7302–7311 (2010).
[88]L. C. Jacobson and V. Molinero, "Can amorphous nuclei grow crystalline clathrates? The size and crystallinity of critical clathrate nuclei," J. Am. Chem. Soc. **133**, 6458–6463 (2011).
[89]L. Jiao, Z. Wang, J. Li, P. Zhao, and R. Wan, "Stability and dissociation studies of CO_2 hydrate under different systems using molecular dynamic simulations," J. Mol. Liq **338**, 116788 (2021).
[90]X. Hao, C. Li, Q. Meng, J. Sun, L. Huang, Q. Bu, and C. Li, "Molecular dynamics simulation of the three-phase equilibrium line of CO_2 hydrate with opc water model," ACS omega **8**, 39847–39854 (2023).
[91]N. Qiu, X. Bai, N. Sun, X. Yu, L. Yang, Y. Li, M. Yang, Q. Huang, and S. Du, "Grand canonical monte carlo simulations on phase equilibria of methane, carbon dioxide, and their mixture hydrates," J. Phys. Chem. B **122**, 9724–9737 (2018).
[92]L. Wang and P. G. Kusalik, "Understanding why constant energy or constant temperature may affect nucleation behavior in MD simulations: A study of gas hydrate nucleation," J. Chem. Phys. **159**, 184501 (2023).
[93]S. Liang and P. G. Kusalik, "Exploring nucleation of H_2S hydrates," Chem. Sci. **2**, 1286–1292 (2011).
[94]S. Liang and P. G. Kusalik, "Nucleation of gas hydrates within constant energy systems," J. Phys. Chem. B **117**, 1403–1410 (2013).
[95]M. H. Waage, T. J. H. Vlugt, and S. Kjelstrup, "Phase diagram of methane and carbon dioxide hydrates computed by Monte Carlo simulations," J. Phys. Chem. B **121**, 7336–7350 (2017).
[96]Y.-T. Tung, L.-J. Chen, Y.-P. Chen, and S.-T. Lin, "Growth of structure i carbon dioxide hydrate from molecular dynamics simulations," J. Phys. Chem. C **115**, 7504–7515 (2011).
[97]O. L. Roberts, E. R. Brownscombe, and L. S. Howe, Oil Gas J. **39**, 37 (1940).
[98]W. M. Deaton and E. M. J. Frost, "Gas hydrates and their relation to the operation of natural-gas pipe lines," U.S. Bureau of Mines Monograph **8**, 101 (1946).
[99]H. H. Reamer, F. T. Selleck, and B. H. Sage, "Some properties of mixed paraffinic and olefinic hydrates," Pet. Trans. AIME **195**, 197–202 (1952).
[100]T. J. Galloway, W. Ruska, P. S. Chappelear, and R. Kobayashi, "Experimental measurement of hydrate numbers for methane and ethane and comparison with theoretical values," Ind. Eng. Chem. Fundamen. **9**, 237–243 (1970).
[101]B. J. Falabella and M. M. Vanpee, "Experimental determination of gas hydrate equilibrium below the ice point," Ind. Eng. Chem. Fund. **13**, 228–231 (1974).
[102]G. D. Holder and G. C. Grigoriou, "Hydrate dissociation pressures of (methane + ethane + water) existence of a locus of minimum pressures," J. Chem. Thermodyn. **12**, 1093–1104 (1980).
[103]G. D. Holder and J. H. Hand, "Multiple-phase equilibria in hydrates from methane, ethane, propane and water mixtures," AIChE J. **28**, 440–447 (1982).
[104]H.-J. Ng and D. B. Robinson, "Hydrate formation in systems containing methane, ethane, propane, carbon dioxide or hydrogen sulfide in the presence of methanol," Fluid Phase Equil. **21**, 145–155 (1985).
[105]D. Avlonitis, *Multiphase Equilibria in Oil-Water Hydrate Forming Systems*, M.Sc. Thesis, Heriot-Watt University (1988).
[106]K. Y. Song and R. Kobayashi, "Final hydrate stability conditions of a methane and propane mixture in the presence of pure water and aqueous solutions of methanol and ethylene glycol," Fluid Phase Equil. **47**, 295–308 (1989).
[107]S. Nakano, K. Yamamoto, and K. Ohgaki, "Natural gas exploitation by carbon dioxide from gas hydrate fields—high-pressure phase equilibrium for an ethane hydrate system," Proc. Instn. Mech. Engnrs. **212**, 159–163 (1998).
[108]S. O. Yang, *Measurements and Prediction of Phase Equilibria for Water + Natural Gas Components in Hydrate-Forming Conditions*, Ph.D. thesis, Korea University (2000).
[109]K. Morita, S. Nakano, and K. Ohgaki, "Structure and stability of ethane hydrate crystal," Fluid Phase Equil. **169**, 167–175 (2000).
[110]J. L. F. Abascal, E. Sanz, R. G. Fernández, and C. Vega, "A potential model for the study of ices and amorphous water: TIP4P/Ice," J. Chem. Phys. **122**, 234511 (2005).
[111]G. M. Martin and J. I. Siepmann, "Transferable potentials for phase equilibria. 1. united-atom description of n-alkanes," J. Phys. Chem. B **102**, 2569–2577 (2001).
[112]M. S. Shah, J. I. Siepmann, and M. Tsapatsis, "Transferable potentials for phase equilibria. improved united-atom description of ethane and ethylene," AIChE Journal **63**, 5098–5110 (2017).
[113]U. Essmann, L. Perera, M. L. Berkowitz, T. Darden, H. Lee, and L. G. Pedersen, "A smooth particle mesh Ewald method," J. Chem. Phys. **103**, 8577–8593 (1995).
[114]J. Algaba, C. Romero-Guzmán, M. J. Torrejón, and F. J. Blas, "Prediction of the univariant two-phase coexistence line of the tetrahydrofuran hydrate from computer simulation," J. Phys. Chem. **160**, 164718 (2024).
[115]V. K. Michalis, I. G. Economou, A. K. Stubos, and I. N. Tsimpanogiannis, "Phase equilibria molecular simulations of hydrogen hydrates via the direct phase coexistence approach," J. Chem. Phys. **157**, 154501 (2022).
[116]J. Costandy, V. K. Michalis, I. N. Tsimpanogiannis, A. K. Stubos, and I. G. Economou, "The role of intermolecular interactions in the prediction of the phase equilibria of carbon dioxide hydrates," J. Chem. Phys. **143**, 094506 (2015).
[117]S. Blazquez, J. Algaba, J. M. Míguez, C. Vega, F. J. Blas, and M. M. Conde, "Three-phase equilibria of hydrates from computer simulation. I: Finite-size effects in the methane hydrate," J. Chem. Phys. **160**, 164721 (2024).
[118]V. Buch, P. Sandler, and J. Sadlej, "Simulations of H_2O solid, liquid, and clusters, with an emphasis on ferroelectric ordering transition in hexagonal ice," J. Phys. Chem. B **102**, 8641–8653 (1998).
[119]J. D. Bernal and R. H. Fowler, "Simulations of H_2O solid, liquid, and clusters, with an emphasis on ferroelectric ordering transition in hexagonal ice," J. Chem. Phys. **1**, 515–548 (1933).
[120]M. A. Cuendet and W. F. V. Gunsteren, "On the calculation of velocity-dependent properties in molecular dynamics simulations using the leapfrog integration algorithm," J. Chem. Phys. **127**, 184102 (2007).
[121]G. Bussi, D. Donadio, and M. Parrinello, "Canonical sampling through velocity rescaling," J. Chem. Phys. **126**, 014101–1–014101–7 (2007).
[122]M. Parrinello and A. Rahman, "Polymorphic transitions in single crystals: A new molecular dynamics method," J. Appl. Phys. **52**, 7182–7190 (1981).
[123]Y. P. Handa, "Compositions, enthalpies of dissociation, and heat capacities in the range 85 to 270 K for clathrate hydrates of methane, ethane, and propane, and enthalpy of dissociation of isobutane hydrate, as determined by a heat-flow calorimeter," J. Chem. Thermodynamics **18**, 915–921 (1986).
[124]J. Qin and W. F. Kuhs, "Quantitative analysis of gas hydrates using raman spectroscopy," AIChE Journal. **59**, 2155–2167 (2013).
[125]K. A. Udachin, C. I. Ratcliffe, and J. A. Ripmeester, "Single crystal diffraction studies of structure I, II and H hydrates: Structure, cage occupancy and composition," J. Supramol. Chem. **2**, 405–408 (2002).
[126]S. Takeya, K. A. Udachin, I. L. Moudrakovski, R. Susilo, and J. A. Ripmeester, "Direct space methods for powder X-ray diffraction for guest-host materials: Applications to cage occupancies and guest distributions in clathrate hydrates," J. Am. Chem. Soc. **132**, 524–531 (2010).